HHS Public Access

Author manuscript

Nat Chem Biol. Author manuscript; available in PMC 2021 November 25.

Published in final edited form as:

Nat Chem Biol. 2021 June ; 17(6): 711–717. doi:10.1038/s41589-021-00802-w.

Acute pharmacological degradation of Helios destabilizes regulatory T cells

Eric S. Wang[#1,2], **Alyssa L. Verano**[#1,2], **Radosław P. Nowak**[#1,2], **J. Christine Yuan**[#1,2], **Katherine A. Donovan**[1,2], **Nicholas A. Eleuteri**[1], **Hong Yue**[1,2], **Kenneth H. Ngo**[3], **Patrick H. Lizotte**[3], **Prafulla C. Gokhale**[3], **Nathanael S. Gray**[1,2,*], **Eric S. Fischer**[1,2,*]

[1]Department of Cancer Biology, Dana-Farber Cancer Institute, Boston MA.

[2]Department of Biological Chemistry and Molecular Pharmacology, Harvard Medical School, Boston, MA.

[3]Belfer Center for Applied Cancer Science, Dana-Farber Cancer Institute, Boston, MA.

[#] These authors contributed equally to this work.

Abstract

The zinc finger transcription factor Helios is critical for maintaining the identity, anergic phenotype, and suppressive activity of regulatory T cells. While it is an attractive target to enhance the efficacy of currently approved immunotherapies, no existing approaches can directly modulate Helios activity or abundance. Here, we report the structure-guided development of small molecules that recruit the E3 ubiquitin ligase substrate receptor Cereblon to Helios, thereby promoting its degradation. Pharmacological Helios degradation destabilized the anergic phenotype and reduced the suppressive activity of regulatory T cells, establishing a route towards Helios-targeting therapeutics. More generally, this study provides a framework for the development of small molecule degraders for previously unligandable targets by reprogramming E3 ligase substrate specificity.

Graphical Abstract

[*]Correspondence to: Nathanael S. Gray (nathanael_gray@dfci.harvard.edu); Eric S. Fischer (eric_fischer@dfci.harvard.edu).

Author contributions: ESW performed the immunoblotting, flow cytometry, and pharmacodynamic experiments. ALV designed and synthesized all compounds. JCY and RPN designed, constructed and JCY performed the biochemical TR-FRET and cellular reporter assays. RPN and JCY conducted protein purification and crystallization, and RPN collected, processed, and refined X-ray data. KAD and NAE conducted the mass spectrometry experiments. HY helped with protein purification and TR-FRET assays. KHN, PHL, and PCG performed the pharmacodynamic experiments. ESW, ALV, and RPN wrote the manuscript. NSG and ESF supervised all aspects of the project. All authors read, revised, and approved the manuscript.

Data and materials availability: All data supporting the findings in this study are provided in the main text and supplementary materials. Structural coordinates are deposited in the protein data bank and available under accession number (PDB: 7LPS). Mass spectrometry raw data files have been deposited in the PRIDE Archive (PXD016168 and PXD023691) for ALV1 and ALV2. The Uniprot human database was used for proteomics analysis.

Code availability: The code necessary to reproduce the statistical analysis for quantitative proteomics can be found at: https://github.com/fischerlab/.

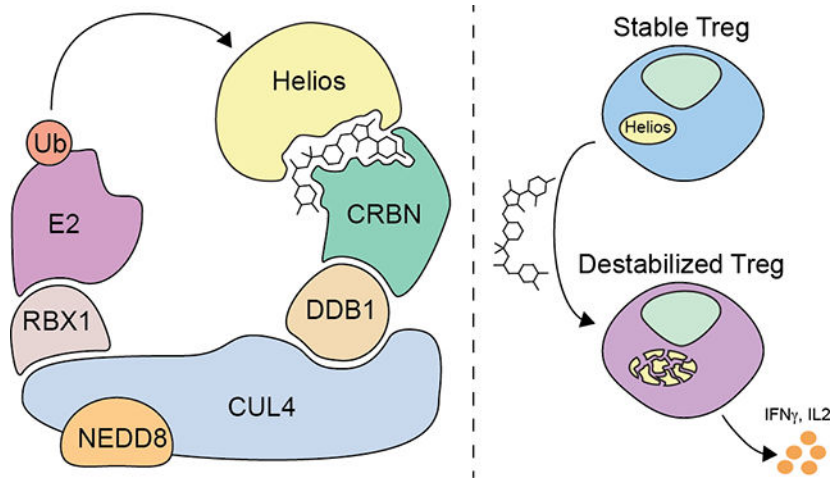

Introduction

Regulatory T cells (Tregs) are a specialized subset of CD4+ T cells that maintain normal immune tolerance and homeostasis but also repress the anti-tumor immune response[1,2]. While antibody-mediated Treg depletion induces regression in a variety of inoculated syngeneic tumors[3], systemic depletion of Tregs provokes autoimmune reactions[4], thereby narrowing the therapeutic window of such approaches.

The transcription factor Helios (IKZF2) is critically required to maintain a stable Treg phenotype in the inflammatory tumor microenvironment. Helios-deficient Tregs lose their suppressive activity and instead acquire effector T cell functions (i.e. secretion of IFNγ), and tumor growth is significantly suppressed in murine tumor models in the context of Helios-deficient Tregs[5–7]. This phenotypic destabilization preferentially occurs in tumor-infiltrating Tregs, which suggests that pharmacologically targeting Helios may mitigate the risk of autoimmunity.

While Helios is an attractive immune-oncology target, transcription factors are traditionally considered to be hard to drug, and no Helios-targeting small molecules have been reported. However, the emerging use of small molecules to induce the ubiquitination and subsequent proteasomal degradation of proteins of interest, referred to as targeted protein degradation, has the potential to expand the druggable proteome. Indeed, thalidomide analogs (also known as IMiDs, or immunomodulatory imide drugs) can induce the degradation of a variety of proteins, such as Ikaros (IKZF1) and Aiolos (IKZF3)[8,9], casein kinase 1α (CK1α)[10], ZFP91[11], SALL4[12,13], and GSPT1[14]. Here, we demonstrate the feasibility of exploiting targeted protein degradation approaches to re-direct an E3 ubiquitin ligase to the transcription factor Helios.

Results

Developing Helios degraders by diversifying the imide core

We sought to pharmacologically reprogram the CUL4-DDB1-RBX1-CRBN ($CRL4^{CRBN}$) ubiquitin ligase towards Helios, a member of the Ikaros transcription factor family[15,16]. Within the Ikaros family, only Ikaros and Aiolos are degraded by canonical imide compounds. The presence of a glutamine residue in the second zinc finger domain in Ikaros and Aiolos enables imide-induced degradation, while the histidine residues in Helios and Eos (IKZF4) and arginine residue in Pegasus (IKZF5) (Extended Data Fig. 1a) are not permissive of imide-induced degradation[8,14]. Interestingly, the imide analog CC-885 induces weak interactions between CRBN and Q146H-IKZF1[14], resulting in minimal degradation (Extended Data Fig. 1b), suggesting that imide analogs may be able to induce Helios degradation. However, in addition to weak Helios binding, CC-885 degrades GSPT1[14,17], a regulator of translation, and is highly cytotoxic (Extended Data Fig. 1c, 2c).

While the Q146H-Ikaros mutant has reduced imide-induced CRBN binding, the Q146A-Ikaros mutant has similar CRBN binding as wildtype Ikaros[14], suggesting that steric or electronic hindrance by the histidine residue, and not loss of interactions with the glutamine, drives decreased CRBN binding affinity. We hypothesized that a more flexible CRBN-binding core compared to imides could accommodate the key histidine residue in Helios, and thus generated ALV-02–146-03 **(1)**, an analog with an expanded anilinomaleimide in place of the standard isoindolinone core (Extended Data Fig. 2a). After verifying that this analog engaged CRBN in cells (Extended Data Fig. 2b), we screened a small, focused library of anilinomaleimides using a CRBN-Helios time-resolved fluorescence energy transfer (TR-FRET) dimerization assay, and iterative rounds of medicinal chemistry optimization led to the discovery of ALV1 **(2)** and ALV2 **(3)** (Fig. 1a).

Both ALV1 and ALV2 bound CRBN in vitro with greater potency than lenalidomide **(4)** but less than CC-885 **(5)** (Fig. 1b), and both compounds also induced CRBN-Helios dimerization in the TR-FRET assay, with greater activity than either CC-885 (positive control) or lenalidomide (negative control) (Fig. 1c). After verifying that these compounds bound to CRBN in cells (Extended Data Fig. 2b), we quantified their degradation activities for Ikaros, Helios, and the anti-target GSPT1 in reporter cells that stably express EGFP fusions of each target followed by P2A splice site-separated mCherry, allowing for ratiometric quantitation of degradation. Our medicinal chemistry campaign optimized for compounds with distinct pharmacological degradation profiles, resulted in the development of ALV1, which degraded both Ikaros and Helios, and ALV2, which exhibited relative selectivity for Helios. Neither ALV1 nor ALV2 destabilized GSPT1, and as expected, lenalidomide only induced degradation of Ikaros, while CC-885 induced degradation of both Ikaros and GSPT1 (Extended Data Fig 2c).

ALV2 is a potent and selective Helios degrader

We next sought to confirm whether ALV1 and ALV2 could destabilize endogenous, untagged proteins. Exposure of Jurkat cells to ALV1 induced degradation of both Ikaros and Helios and treatment with ALV2 preferentially induced degradation of Helios, while neither

compound affected the stability of GSPT1 (Fig. 1d). As expected, either CRBN deficiency or co-administration of the proteasome inhibitor carfilzomib prevented degradation (Fig. 1d, e). To globally assess the selectivity of ALV1 and ALV2, we performed multiplexed mass spectrometry-based proteomic analysis of Jurkat cells following 4h treatment (Fig. 1f, Supplementary Data Set 1). Across ~7,900 quantified proteins, we found that both ALV1 and ALV2 were highly potent for inducing Helios degradation without unexpected off-target activity (Supplementary Table 1). In addition to Ikaros family members, we observed potent degradation of ZNF692 and ZNF653, common imide degradation targets[12], and identified ZNF324 as a potential novel target of ALV2 (Extended Data Fig. 3). Thus, proteome-wide analysis revealed that the nonselective compound ALV1 exhibited similar degradation activity towards IKZF1/2/3 while ALV2 preferentially promoted Helios degradation, as also observed by immunoblot.

Structural basis of ALV1 induced Helios/CRBN dimerization

To understand the structural basis for small molecule-mediated recruitment of Helios to CRBN, we reconstituted the complex of hsDDB1ΔB (DDB1 with an internal deletion of the flexible BPB domain[18]), hsCRBN, and hsIKZF2^{ZnF2} in the presence of ALV1. Crystals were obtained for the 152.8 kDa complex, and its structure was determined to 3.8 Å resolution (Fig. 2a, Supplementary Table 2). The DDB1-CRBN complex resembles previously described structures[18], and DDB1ΔB did not interact with IKZF2^{ZnF2} (Fig. 2a, b). CRBN was observed in a closed conformation, where the N-terminal domain (NTD), C-terminal domain (CTD), and helical-bundle domain (HBD) of CRBN form a tight interface[19,20]. IKZF2^{ZnF2} interacts with the CRBN CTD through the β-hairpin loop and the C-terminal α-helix. The glutarimide moiety of ALV1 binds the canonical triple tryptophan imide pocket, with the maleimide core and the 3-chloro-4-methylphenyl ‘tail’ positioned away from the zinc finger to interact with CRBN CTD H353, P352 and NTD F102 (Fig. 2b). The interface between ALV1 and the IKZF2^{ZnF2} β-hairpin loop (IKZF2 residues 143–145) is mediated by the central aniline and olefin of the maleimide core. While the modest resolution of 3.8 Å prevents detailed analysis, we note that H141 of IKZF2, the residue that controls sensitivity of IKZF1/2 to imide-induced degradation, is in close proximity (~3.5Å) to the ethylbenzene moiety of ALV1, potentially contributing hydrophobic interactions.

IKZF2^{ZnF2} is positioned similarly to IKZF1^{ZnF2} in a previously reported structure of the DDB1-CRBN-pomalidomide complex bound to IKZF1^{ZnF2} (PDB: 6H0F), with a 0.7 Å translation across the α-helix (Fig. 2c). In contrast, when compared to the crystal structure of DDB1-CRBN-CC-885-GSPT1 (PDB: 5HXB), ALV1 is bound in a groove explored by CC-885 but with noticeably different location of the common 3-chloro-4-methylphenyl tail, which would clash with V536 of GSPT1 (Fig. 2d). The hydrophobic ethylbenzene moiety of ALV1, as compared to the urea moiety of CC-885, was in close proximity to GSPT1 Q534 with potential for steric clash (Fig. 2d), providing a structural rationale for the inability of ALV1 and ALV2 to degrade GSPT1.

Degradation of Helios de-represses expression of IL2

While the direct transcriptional targets of Helios have not been fully elucidated, Helios has been reported to negatively regulate *Il2* expression, as transient knockdown of Helios

promotes IL-2 expression in Tregs, while forced expression of Helios in CD4+ FoxP3- T cells diminishes their ability to produce IL-2[21]. We assessed the effects of ALV1 and ALV2 treatment on the elaboration of IL-2 from stimulated Jurkat cells (Extended Data Fig. 4). As expected, lenalidomide enhanced IL-2 secretion, as Ikaros and Aiolos are also known negative regulators of *Il2*[22–24]. Consistent with the ascribed role of Helios in suppressing IL-2, both ALV1 and ALV2 promoted IL-2 secretion to a greater extent than lenalidomide, suggesting that Helios more strongly represses IL-2 production than Ikaros/Aiolos in this context. IL-2 therefore serves as a proximal pharmacological marker of Helios degradation.

Pharmacological Helios degradation in CRBN$^{I391V/I391V}$ mice

While genetically encoded Helios deficiency in murine Tregs throughout their development results in destabilization of the anergic Treg phenotype[5,6], it was unknown whether acute Helios degradation would have a similar effect. Imides do not induce IKZF1/3 degradation in wildtype mice due to a single amino acid difference between human and murine CRBN, which interferes with interactions between CRBN and IKZF1/3[10]. Thus, we first tested our selective Helios degrader in cells derived from a humanized knock-in *Crbn*$^{I391V/I391V}$ mouse that is permissive for imide-induced IKZF1/3 degradation[25].

In both wildtype and *Crbn*$^{I391V/I391V}$ mice, Ikaros was highly expressed in conventional CD4+ and CD8+ T cells, while Helios was primarily expressed in FoxP3+ CD4+ Tregs (Extended Data Fig. 5). In *Crbn*$^{I391V/I391V}$ but not wildtype cells, lenalidomide treatment induced selective degradation of Ikaros, while ALV2 treatment destabilized Helios (Extended Data Fig. 5), consistent with the previously observed selectivity profiles of these two compounds. Next, we treated *Crbn*$^{I391V/I391V}$ Tregs (isolated CD4+ CD25+ cells) with ALV2 or DMSO control for 4 days under inflammatory conditions (5 ng/ml IL-2 + 20 ng/ml IL-4), as previously described[5], and found that ALV2-treated FoxP3+ Tregs expressed significantly lower levels of Helios than vehicle-treated FoxP3+ Tregs (Extended Data Fig. 6a). Moreover, restimulation of cells with PMA/ionomycin induced a significantly higher percentage of IFNγ-producing Tregs in ALV2-treated compared to vehicle-treated Foxp3+ Tregs (Extended Data Fig. 6b), consistent with *Ikzf2*$^{-/-}$ Tregs acquiring effector functions, which demonstrates that acute pharmacologic degradation of Helios can recapitulate its genetic loss in murine Tregs. Finally, we administered ALV2 or vehicle control to *Crbn*$^{I391V/I391V}$ mice and found that ALV2 treatment reduced Helios but not Ikaros levels in splenic CD4+ FoxP3+ Tregs (Extended Data Fig. 6c, Supplementary Table 3), demonstrating that ALV2 can induce selective Helios degradation *in vivo*.

Acute Helios degradation destabilizes human Tregs ex vivo

The differential pharmacology of imide molecules between mice and human[12,13] results in an absence of mouse models that would meaningfully recapitulate the immunomodulatory pharmacology of imides such as ALV2; consequently, *ex vivo* models of human origin are commonly utilized for pre-clinical development of thalidomide derivatives. We therefore utilized Tregs isolated from human peripheral blood to test the effects of ALV1 and ALV2 *ex vivo*. Consistent with our previous results, ALV1 potently induced degradation of both Ikaros and Helios, while ALV2 selectively destabilized Helios (Fig. 3a). Like Helios, Eos (IKZF4) also encodes a histidine residue at the position critical for controlling sensitivity to

imide-mediated degradation (Extended Data Fig. 1a) and would be predicted to be sensitive to ALV1 and ALV2. As Eos is not expressed in Jurkat cells and thus could not be detected by immunoblot or proteomics (Fig. 1), we assessed the effects of ALV1 and ALV2 on endogenous Eos levels in human Tregs by flow cytometry and found that both compounds induced Eos degradation. Of note, Eos has similar regulatory functions in Tregs as Helios, as knockdown or deletion of Eos disrupt the canonical suppressive phenotype of Tregs[26,27]. As small molecule degraders can exhibit different selectivity profiles in different cell types[28], we assessed the selectivity of ALV1 and ALV2 in human Tregs expanded *ex vivo* via multiplexed mass spectrometry-based proteomic analysis (Fig. 3b). Across ~6,800 quantified proteins, we found that ALV1 potently reduced the protein abundance of IKZF1–4, while ALV2 preferentially degraded IKZF2/4, consistent with our previous results. The hallmark Treg transcription factor FoxP3 was detected but its levels were not affected during this short treatment regimen (Fig. 3c). In addition to Ikaros family members, we observed potent degradation of ZMYM2 in both ALV1- and ALV2-treated human Tregs, while ALV1 treatment also reduced the abundance of CK1α (CSNK1A1), a known lenalidomide target[10], as well as the ribosomal protein RPL4. Thus, proteome-wide analysis in human Tregs revealed that the nonselective compound ALV1 exhibited pan-Ikaros family degradation activity while ALV2 preferentially promoted Helios/Eos degradation, with minimal additional degradation targets.

We next assessed the phenotypic consequences of Helios/Eos degradation in human Tregs. Consistent with the loss of Treg anergy observed in murine cells, PMA/ionomycin restimulation of human Tregs expanded in the presence of ALV2 significantly increased the percentage of IL-2 or IFNγ-producing Tregs over vehicle control (Fig. 4a, b). We also found that human Tregs expanded in the presence of ALV2 were less able to repress the proliferation of responder cells (Fig. 4c). Thus, acute pharmacological loss of Helios/Eos promotes loss of Treg anergy and diminishes their suppressive activity.

Discussion

Here, we describe the development of novel small molecule ligands of CRBN capable of inducing degradation of Helios, one of which exhibited relative selectivity for Helios over Ikaros/Aiolos, the classic neo-substrates of imide compounds. Notably, the preferential Helios degrader ALV2 destabilized the anergic phenotype of regulatory Tregs, consistent with previously reported phenotypes of *Ikzf2−/−* Tregs[5,6,29], demonstrating that acute pharmacological degradation of Helios recapitulates the phenotype of genetic loss of *Ikzf2* in Tregs. Thus, our data suggest that Helios-mediated regulation of Treg stability is not established during thymic and/or peripheral Treg development, and provides a roadmap for the development of Helios-degrading therapeutics as immunotherapy agents that may synergize with immune checkpoint blockade.

Eos, another member of the Ikaros transcription factor family, also encodes a histidine at the same position as Helios within the critical zinc finger domain that regulates the degradability of this family of proteins. As expected, the novel Helios degraders described here also potently destabilize Eos in human Tregs, underscoring the selective targeting of this critical histidine residue. As genetic studies suggest that Eos has a similar function to Helios in

terms of maintaining the regulatory T cell phenotype[26,27], targeting both Helios and Eos may result in enhanced Treg destabilization.

We demonstrate that maintaining the core glutarimide pharmacophore but reducing the rigidity of the phthalamide moiety results in compounds that accommodate differences in amino acid sequence of the neosubstrate β-hairpin loop. Proteomic analysis identified C_2H_2 transcription factor ZNF324 as a novel neosubstrate of CRBN degraded by ALV2. ZNF324 harbors 10 C_2H_2 zinc-finger domains, 8 of which contain the CxxCG motif permissive of IMiD mediated degradation[20]. Notably none of the 8 zinc fingers contains Q present in QCxxCG of IKZF1/3 or H present in IKZF2^{ZnF2}; instead, this position consists of A/V/E/R. While the degron motif of ZNF324 remains to be identified, the VCxxCG degron has previously been established in thalidomide-mediated degradation of SALL4$^{ZnF2\ 12}$ and is a candidate degron for ZNF324. Small changes in ligand conformation in this region could significantly affect ternary complex stability and therefore impact degradation.

The observed preference of ALV2 for degradation of IKZF2 over IKZF1/3 suggests that ALV1 but not ALV2 tolerate the additional bulk of glutamine over histidine residues, but detailed insights into the drivers of selectivity will require further structures of these molecules in complex with IKZF1/3. As the structural data suggest that the zinc-finger binding mode, which is dominated by backbone interactions, can undergo local rearrangements/breathing, we imagine that more diverse chemical libraries will enable broad targeting of β-hairpin containing targets beyond the canonical C_2H_2 zinc finger. Thus, similar efforts may yield small molecule degraders for other previously undruggable protein targets.

Experimental Materials and Methods

Compounds

Lenalidomide (HY-A0003, MedChemExpress), CC-885 (19966, Cayman chemical), carfilzomib (ab216469, Abcam) were purchased from the indicated vendors and subjected to in-house LC-MS for quality control.

Western blots and antibodies

Cells were lysed in M-PER buffer (Thermo Scientific) containing protease/phosphatase inhibitor cocktail (Roche). After assessing protein concentration by BCA assay (Pierce), equal amounts of protein for each sample were loaded into 4–12% Bis-Tris gels (Invitrogen), transferred to nitrocellulose membranes, and immunoblotted with antibodies against Ikaros, Helios, cleaved Caspase-3, and Actin (Cell Signaling); and eRF3/GSPT1 (Abcam). Membranes were detected on an Odyssey detection system (LI-COR Biosciences) after incubation with IRDye®800-labeled goat anti-rabbit IgG and IRDye®680-labeled goat anti-mouse IgG (LI-COR) secondary antibodies.

Cell culture

FLP293T derived stable cell lines were cultured in DMEM supplemented with 10% dialyzed fetal bovine serum (FBS). Wildtype and *Crbn−/−* Jurkat cells were cultured in RPMI

supplemented with 10% FBS and 1% penicillin/streptomycin in a 37°C incubator with 5% CO_2. CD4+ CD25+ regulatory T cells were purified from spleens from wildtype or *Crbn*$^{I391V/I391V}$ mice using the EasySep Mouse CD4+ CD25+ Regulatory T cell Isolation Kit (StemCell Technologies). T cells were cultured in RPMI supplemented with 10% FBS, 1% penicillin/streptomycin, 1% non-essential amino acids, 1% sodium pyruvate, 2 mM GlutaMax, 10 mM HEPES, and 50 μM 2-mercaptoethanol, as well as 5 ng/ml recombinant murine IL-2 (Biolegend) and 20 ng/ml recombinant murine IL-4 (Biolegend). Human regulatory T cells were isolated from peripheral blood mononuclear cells using the EasySep Human $CD4^+CD127^{low}CD25^+$ Regulatory T Cell Isolation Kit (StemCell Technologies) and expanded for 12–14 days in the presence of 500 U/ml human IL-2, Immunocult CD3/CD28 T cell activator (StemCell Technologies), and compound in ImmunoCult-XF T Cell Expansion Medium (StemCell Technologies). Cells were stimulated with 1X PMA/ionomycin (Biolegend) for 1h followed by the addition of brefeldin A (Biolegend) for another 3h.

Flow cytometry

Live cells were determined by Zombie® fixable NIR dead cell stain kit (Biolegend). Cell pellets were re-suspended in PBS with 2% FBS for Fluorescence-activated cell sorting (FACS) analysis. Cells were surface stained, fixed/permeabilized using the FoxP3 / Transcription Factor Staining Buffer (eBioscience), and then intracellular stained as indicated with different combinations of fluorochrome-coupled antibodies against: CD3 (clone 17A2), TCRβ (clone H57–597), CD4 (clone GK1.5), CD8 (clone 53–6.7), Foxp3 (clone MF-14), Ikaros (clone 2A9/Ikaros), and interferon γ (clone XMG1.2); human CD3 (clone OKT3 or HIT3a), CD4 (clone OKT4), FoxP3 (clone 206D), Ikaros (clone 16B5C71), Eos (clone W16032B), IL-2 (clone MQ1–17H12), and interferon γ (clone 4S.B3); mouse/human Helios (clone 22F6); or mouse IgG1,κ (clone MOPC-21), hamster IgG (clone HTK888), mouse IgG2a,κ (clone MOPC-173), and rat IgG2a,κ (clone RTK2758) isotype controls, all from Biolegend. Antibodies were diluted at 1:100. Cells were imaged on a BD LSRFortessa (BD Biosciences) and analyzed using FlowJo software (Tree Star). FACS gating strategies are illustrated in Extended Data Fig. 7.

Treg suppression assay

Human Tregs expanded for 12–14d in the presence of 1 μM ALV2 or vehicle control were incubated with CellTrace Violet (CTV)-labeled autologous CD3+ human T cells at several different Treg:Tresp ratios, Immunocult CD3/CD28 T cell activator, and 1 μM ALV2 or vehicle control in compound in ImmunoCult-XF T Cell Expansion Medium for 5d. Cell division profiles were evaluated by flow cytometry after staining for CD3, CD4, and CD8.

IL-2 ELISA

Jurkat cells were pre-treated with 1 μM of the indicated compounds for 18h, and then stimulated with Immunocult T cell activator (StemCell Technologies) for 24h. IL-2 levels in the supernatant were analyzed by AlphaLISA (Perkin Elmers) according to the manufacturer's protocol.

Pharmacodynamic studies

Crbn$^{I391V/I391V}$ mice were treated with vehicle (10% DMSO / 50% PEG400 / 40% water) or ALV2 (100 mg/kg via intraperitoneal injection twice daily) for 7d. Spleens were collected 4h after the final treatment. All *in vivo* studies were conducted at Dana-Farber Cancer Institute with the approval of the Institutional Animal Care and Use Committee in an AAALAC accredited vivarium. Mice were housed in individually ventilated cages in a state-of-the-art OptiMICE rack system equipped with automatic watering. The vivarium is temperature controlled (72 ± 2° F) and a target range of 35–55% relative humidity, with automated lighting ensuring a standard 12:12 hour light/dark circadian cycle.

Constructs and protein purification

Wild-type and mutant versions of human DDB1, human CRBN, human IKZF1Δ (residues 83–193,239–255), human IKZF2Δ (residues 78–191,241–257) and human IKZF2^{ZnF2} (residues 136–164) were cloned in pAC-derived vectors[31] and recombinant proteins were expressed as N-terminal TEV cleavable His_6 (DDB1ΔB, CRBN), StrepII-Avi (IKZF1Δ), StrepII-Avi (IKZF2Δ), StrepII-Avi (IKZF2^{ZnF2}), StrepII-Avi (CRBN) or Flag-Spy (CRBN)[32] fusions in *Trichoplusia ni* High-Five insect cells using the baculovirus expression system (Invitrogen). Cells were lysed in the presence of 50 mM Tris-HCl pH 8.0, 200 mM NaCl, 1 mM TCEP, 1 mM PMSF and 1x protease inhibitor cocktail (Sigma). Following ultracentrifugation, the soluble fraction was passed over appropriate affinity resin Strep-Tactin Sepharose (IBA), Ni Sepharose 6 Fast Flow affinity resin (GE Healthcare) or Flag-M2 sepharose and eluted with wash buffer (50 mM Tris-HCl pH 8.0, 200 mM NaCl, 1 mM TCEP) supplemented with 50 mM Biotin (IBA), 100 mM imidazole (Fischer Chemical) or Flag peptide respectively. The affinity-purified protein was either further purified (His_6CRBN-His_6DDB1ΔB or StrepII-Avi-CRBN-His_6DDB1ΔB) via ion exchange chromatography (Poros 50HQ) and subjected to size exclusion chromatography or directly covalently labelled with BODIPY-FL-SpyCatcher$_{S50C}$(Flag-Spy-CRBN-His_6-Spy-DDB1ΔB) as previously described[19] and subjected to size exclusion chromatography or TEV cleaved overnight (IKZF2^{ZnF2}) and subjected to size exclusion chromatography or biotinylated overnight concentrated and directly subjected to size exclusion chromatography (IKZF1Δ, IKZF2Δ, StrepII-Avi-CRBN-His_6DDB1ΔB) in 50 mM HEPES pH 7.4, 200 mM NaCl and 1 mM TCEP. Biotinylation of IKZF1Δ, IKZF2Δ variants was performed as previously described[33].

The protein-containing fractions were concentrated using ultrafiltration (Millipore) and flash frozen in liquid nitrogen (his-spy-DDB1ΔB-his-CRBN at ~60 μM, BODIPY-FL-SpyCatcher$_{S50C}$(Flag-Spy-CRBN-His_6-Spy-DDB1ΔB) at ~5–15 μM, biotinylated StrepII-Avi-CRBN-His_6DDB1ΔB at 3.6 μM, biotinylated StrepII-Avi-IKZF1Δ or StrepII-Avi-IKZF2Δ at ~10–20 μM, IKZF2^{ZnF2} at ~350 μM concentration) and stored at −80°C.

CRBN TR-FRET binding assay

Compounds in binding assay were dispensed into a 384-well microplate containing the assay mix (Corning, 4514) using the D300e Digital Dispenser (HP) normalized to 1% DMSO. Assay mix constituted of 100 nM biotinylated StrepII-Avi-CRBN-His_6DDB1ΔB, 10 nM BODIPY-lenalidomide tracer and 2 nM terbium-coupled streptavidin (Invitrogen) prepared

in assay buffer with 50 mM Tris pH 7.5, 200 mM NaCl, 1 mM TCEP, and 0.1% Pluronic F-68 solution (Sigma). The reactions were incubated for 15 min at room temperature before TR-FRET measurements were conducted. After excitation of terbium fluorescence at 337 nm, emission at 490 nm (terbium) and 520 nm (BODIPY) were recorded with a 70 μs delay over 600 μs to reduce background fluorescence, and the reaction was followed over multiple 60 s cycles of each data point using a PHERAstar FS microplate reader (BMG Labtech) until steady state was reached. The TR-FRET signal was calculated as the 520/490 nm ratio for each data point. IC_{50} values were calculated using the nonlinear fit variable slope model GraphPad Prism 7.

TR-FRET dimerization assay

Compounds in binding assay were dispensed into a 384-well microplate containing the assay mix (Corning, 4514) using the D300e Digital Dispenser (HP) normalized to 1% DMSO. The assay mix contained 100 nM biotinylated strep-avi-IKZF1 or strep-avi-IKZF2, 200 nM His_6-spy-DDB1ΔB-Flag-spy-$CRBN_{Bodipy\text{-}Spycatcher}$ (see figure legends), and 2 nM terbium-coupled streptavidin (Invitrogen) in a buffer composed of 50 mM Tris pH 7.5, 100 mM NaCl, 1 mM TCEP, and 0.1% Pluronic F-68 solution (Sigma). The reactions were incubated for 15 min at room temperature before TR-FRET measurements were conducted. After excitation of terbium fluorescence at 337 nm, emission at 490 nm (terbium) and 520 nm (Bodipy) were recorded with a 70 μs delay over 600 μs to reduce background fluorescence, and the reaction was followed over 30× 200 s cycles of each data point using a PHERAstar FS microplate reader (BMG Labtech). The TR-FRET signal was calculated as the 520/490 nm ratio for each data point. Data from three independent measurements (n=3), each calculated as an average of at least three technical replicates per well per experiment, was plotted and the half-maximal effective concentrations EC_{50} values calculated using nonlinear fit variable slope equation in GraphPad Prism 7.

Crystallization and data collection

We used a previously developed DDB1 construct lacking WD40 propeller B (BPB, residues 396–705) domain (referred to as DDB1ΔB). For crystallization of His_6-DDB1ΔB-His_6-CRBN-ALV1-$IKZF2^{ZnF2}$ 100 μM of ALV1 was mixed with 60 μM $IKZF2^{ZnF2}$ and 60 μM His_6-DDB1ΔB-His_6-CRBN and incubated for 15 min on ice. Crystallization plates were set up in 3 sub-well plates (Intelli, Art Robbins) by vapor diffusion using NT8 (Formulatrix) at 20°C and images acquired using RockImager 1000 (Formulatrix).

Crystals appeared in well H1 of Index HT Screen (Hampton Research) within 1 day and were fully grown after 3–7 days. Thin plate-like crystals were present in condition H1 (0.2 M Magnesium Chloride Hexahydrate, 25% (w/v) PEG3350, 0.1 M Tris pH 8.5) in 2:1 or 1:1 protein to precipitant ratio in 150 nL drops.

Further optimization of condition in Index HT Screen H1 by seeding resulted in optimal crystals in a condition containing 30% (w/v) PEG3350, 0.1 M Tris pH 8.57 in 2:1 protein to precipitant ratio of 150 nL drops.

Crystals were cryo-protected in reservoir solution supplemented with 20% glycerol containing 200 μM ALV1 and flash–cooled in liquid nitrogen. Diffraction data were

collected at the APS Chicago (beamline 24-ID-C) with a Pilatus 6M-F detector at a temperature of 100 K. Data were indexed and integrated using RAPD pipeline (APS Chicago). Data processing statistics, refinement statistics and model quality parameters are provided in Extended Data Table 1.

Structure determination and model building

The DDB1ΔB-CRBN-ALV1- IKZF2^{ZnF2} ternary complex crystallized in space group $P2_1$ with four complexes in the asymmetric unit. PHASER[34] (version: 2.8.3) was used to determine the structures by molecular replacement using a crystallographic model of DDB1ΔB-CRBN based on a crystal structure pdb: 5fqd. The initial model was iteratively improved with COOT (version: 0.9.1) and refined using PHENIX.REFINE[35] (version: 1.17.1–3660) and autoBUSTER (version: 2.10.4) using pdb: 6h0g for reference restraints[36], and with ligand restraints generated by PHENIX.ELBOW[35] (module of PHENIX version: 1.19.1–4122). Protein geometry analysis revealed 0.60%, Ramachandran outliers, with 95.72% residues in favored regions and 3.68% residues in allowed regions for the complex with ALV1. Figures were generated with PyMOL (The PyMOL Molecular Graphics System, version 1.8.6.0 Schrödinger, LLC) and model quality was assessed with MOLPROBITY[37]. Software used in this project was curated by SBGrid[30].

Cellular degradation assays

IKZF1Δ, IKZF2Δ, GSPT1 were subcloned into mammalian pcDNA5/FRT Vector (Ampicillin and Hygromycin B resistant) modified to contain MCS-eGFP-P2A-mCherry. Stable cell lines expressing eGFP-protein fusion and mCherry reporter were generated using Flip-In 293 system. Plasmid (0.3 μg) and pOG44 (4.7 μg) DNA were preincubated in 100 μL of Opti-MEM I (Gibco, Life Technologies) media containing 0.05 mg/ml Lipofectamine 2000 (Invitrogen) for 20 min and added to Flip-In 293 cells containing 1.9 ml of DMEM media (Gibco, Life Technologies) per well in a 6-well plate format (Falcon, 353046). Cells were propagated after 48 h and transferred into a 10 cm^2 plate (Corning, 430165) in DMEM media containing 50 μg/ml of Hygromycin B (REF 10687010, Invitrogen) as a selection marker. Following 2–3 passage cycles, FACS (FACSAria II, BD) was used to enrich for cells expressing eGFP and mCherry.

Cells stably expressing the IKZF1Δ, IKZF2Δ or GSPT1 GFP fusions with mCherry reporter were seeded at 30–50% confluency in 384-well plates with 50 μL FluoroBrite DMEM media (Thermo Fisher Scientific A18967) containing 10% FBS per well a day before compound treatment. Compound titrations were dispensed using a D300e Digital Dispenser (HP), normalized to 0.5% DMSO, and incubated with cells for 5 hours.

The assay plate was imaged immediately using an Acumen High Content Imager (TTP Labtech) with 488 nm and 561 nm lasers in 2 μm x 1 μm grid per well format. The resulting images were analyzed using CellProfiler[38]. A series of image analysis steps (‘image analysis pipeline’) was constructed. First, the red and green channels were aligned and cropped to target the middle of each well (to avoid analysis of heavily clumped cells at the edges), and a background illumination function was calculated for both red and green channels of each well individually and subtracted to correct for illumination variations across the 384-well

plate from various sources of error. An additional step was then applied to the green channel to suppress the analysis of large auto fluorescent artifacts and enhance the analysis of cell specific fluorescence by way of selecting for objects under a given size (30 A.U.) and with a given shape (speckles). mCherry-positive cells were then identified in the red channel filtering for objects between 8–60 pixels in diameter and using intensity to distinguish between clumped objects. The green channel was then segmented into GFP positive and negative areas and objects were labeled as GFP positive if at least 40% of it overlapped with a GFP positive area. The fraction of GFP-positive cells/mCherry-positive cells in each well was then calculated, and the green and red images were rescaled for visualization. The concentrations that lead to half degradation at 5h ($DC_{50,\ 5h}$) were calculated using the nonlinear fit variable slope model in GraphPad Prism 7.

Competitive displacement assay for cellular CRBN engagement

Cells stably expressing the $BRD4_{BD2}$-GFP with mCherry reporter[19] were seeded at 30–50% confluency in 384-well plates with 50 μL FluoroBrite DMEM media (Thermo Fisher Scientific A18967) containing 10% FBS per well a day before compound treatment. Compound titrations and 100 nM dBET6 were dispensed using a D300e Digital Dispenser (HP), normalized to 0.5% DMSO, and incubated with cells for 5 hours. Assay plates were imaged using Acumen (TTP Labtech) as described above. The values for the concentrations that lead to a 50% increase in $BRD4_{BD2}$-eGFP accumulation (EC_{50}) were calculated using the nonlinear fit variable slope model in GraphPad Prism 7.

Sample preparation TMT LC-MS3 mass spectrometry

Experimental methods for were previously reported[28] and summarized briefly as follows. Jurkat cells or human Tregs were treated with DMSO (biological triplicate) or 1 μM of compounds ALV1 or ALV2 for 4 hours, and cells were harvested by centrifugation. Cells were lysed by addition of Urea lysis buffer (8 M Urea, 50 mM NaCl, 50 mM 4-(2hydroxyethyl)-1-piperazineethanesulfonic acid (EPPS) pH 8.5, Protease and Phosphatase inhibitors from Roche) followed by manual homogenization by 20 passes through a 21-gauge (1.25 in. long) needle. Cell lysate was clarified by centrifugation and protein concentration measured by micro-BCA assay (Pierce). 50 – 200 μg of protein for each sample were reduced and alkylated as previously described[12].

Proteins were precipitated using methanol/chloroform, resuspended in 4 M Urea, 50 mM HEPES pH 7.4, followed by dilution to 1 M urea with the addition of 200 mM EPPS, pH 8. Proteins were digested with LysC (1:50; enzyme:protein) for 12 hours at room temperature, followed by dilution to 0.5 M Urea with 200 mM EPPS pH 8 for digestion with trypsin (1:50; enzyme:protein) for 6 hours at 37 °C. Anhydrous ACN was added to each peptide sample to a final concentration of 30% v/v, and Tandem Mass Tag (TMT) labeling reagent (Thermo Fisher Scientific) was added to each sample at a ratio of 1:4 peptide:TMT label and labeling occurred over 1.5 hours at room temperature. The labeling reaction was quenched by the addition of hydroxylamine to a final concentration of 0.3% for 15 minutes at room temperature. Each of the sample channels were then combined in a 1:1 ratio and desalted using in-house C_{18} stage tips, followed by LC-MS analysis for assessment of sample quality and channel ratio comparison. Samples were then combined using the adjusted volumes

determined in the channel ratio analysis, dried down in a speed vacuum and desalted using C_{18} SPE columns (Sep-Pak, Waters). Samples were then offline fractionated into 96 fractions by high pH reverse-phase HPLC (Agilent LC1260) through an aeris peptide xb-c18 column (phenomenex) with mobile phase A containing 5% acetonitrile and 10 mM NH_4HCO_3 in LC-MS grade H_2O, and mobile phase B containing 90% acetonitrile and 5 mM NH_4HCO_3 in LC-MS grade H_2O (both pH 8.0). The 96 resulting fractions were then combined in a non-contiguous manner into 24 fractions and these fractions were used for subsequent mass spectrometry analysis.

Data were collected using either an Orbitrap Fusion Lumos mass spectrometer (Thermo Fisher Scientific, San Jose, CA, USA) coupled with a Proxeon EASY-nLC 1200 LC pump or an Orbitrap Eclipse Tribrid mass spectrometer (Thermo Fisher Scientific, San Jose, CA, USA) coupled with an UltiMate 3000 RSLCnano System. Peptides were separated on an EasySpray ES803a or ES803a.rev2 75 μm inner diameter microcapillary column (Thermo Fisher Scientific). Peptides were separated using a 190 min gradient of 6–27% acetonitrile in 1.0% formic acid with a flow rate of 300 nL/min.

Each analysis used an MS3-based TMT method as described previously[39]. The data were acquired using a mass range of *m/z* 340 – 1350, resolution 120,000, AGC target 5×10^5, maximum injection time 100 ms, dynamic exclusion of 120 seconds for the peptide measurements in the Orbitrap. Data dependent MS2 spectra were acquired in the ion trap with a normalized collision energy (NCE) set at 35%, AGC target set to 1.8×10^4 and a maximum injection time of 120 ms. MS3 scans were acquired in the Orbitrap with a HCD collision energy set to 55%, AGC target set to 2×10^5, maximum injection time of 150 ms, resolution at 50,000 and with a maximum synchronous precursor selection (SPS) precursors set to 10. The Advanced Peak Detection (APD) algorithm was disabled.

LC-MS data analysis

Proteome Discoverer 2.2 or 2.4 (Thermo Fisher Scientific) was used for .RAW file processing and controlling peptide and protein level false discovery rates, assembling proteins from peptides, and protein quantification from peptides. MS/MS spectra were searched against a Uniprot human database (September 2016) with both the forward and reverse sequences. Database search criteria are as follows: tryptic with two missed cleavages, a precursor mass tolerance of 20 ppm, fragment ion mass tolerance of 0.6 Da, static alkylation of cysteine (57.02146 Da), static TMT labelling of lysine residues and N-termini of peptides (229.16293 Da), and variable oxidation of methionine (15.99491 Da). TMT reporter ion intensities were measured using a 0.003 Da window around the theoretical *m/z* for each reporter ion in the MS3 scan. Peptide spectral matches with poor quality MS3 spectra were excluded from quantitation (summed signal-to-noise across 10 channels < 100 and precursor isolation specificity < 0.5), and resulting data was filtered to only include proteins that had a minimum of 3 unique peptides identified. Reporter ion intensities were normalized and scaled using in-house scripts in the R framework (version 4.0.2)[40]. Statistical analysis was carried out using the limma package (version 3.44.3) within the R framework[41]. Significant changes were assessed using a moderated t-test as implemented in Bioconductor's Limma package.

Extended Data

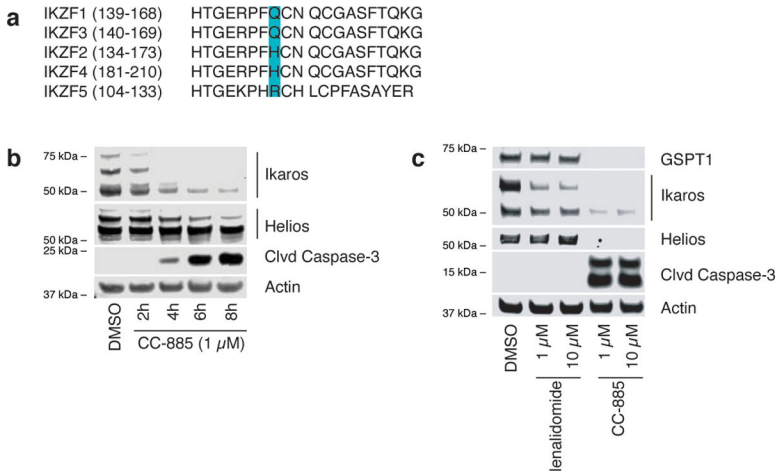

Extended Data Fig. 1. Critical histidine residue in Helios regulates sensitivity to imide-induced degradation

a, Sequence alignment of the second zinc finger domain of Ikaros family proteins, with the residue that controls sensitivity to IMiD-induced degradation (glutamine residue in IKZF1/3, histidine in IKZF2/4) highlighted in cyan. **b,** Immunoblot from Jurkat cells treated as indicated. **c,** Immunoblot from Jurkat cells treated as indicated for 16h. Loss of Helios abundance may be secondary to defects in translation and subsequent initiation of programmed cell death. Data in **b, c** are representative of $n = 2$ independent experiments. Uncropped gels for **c** are included as Source Data – Extended Figure 1.

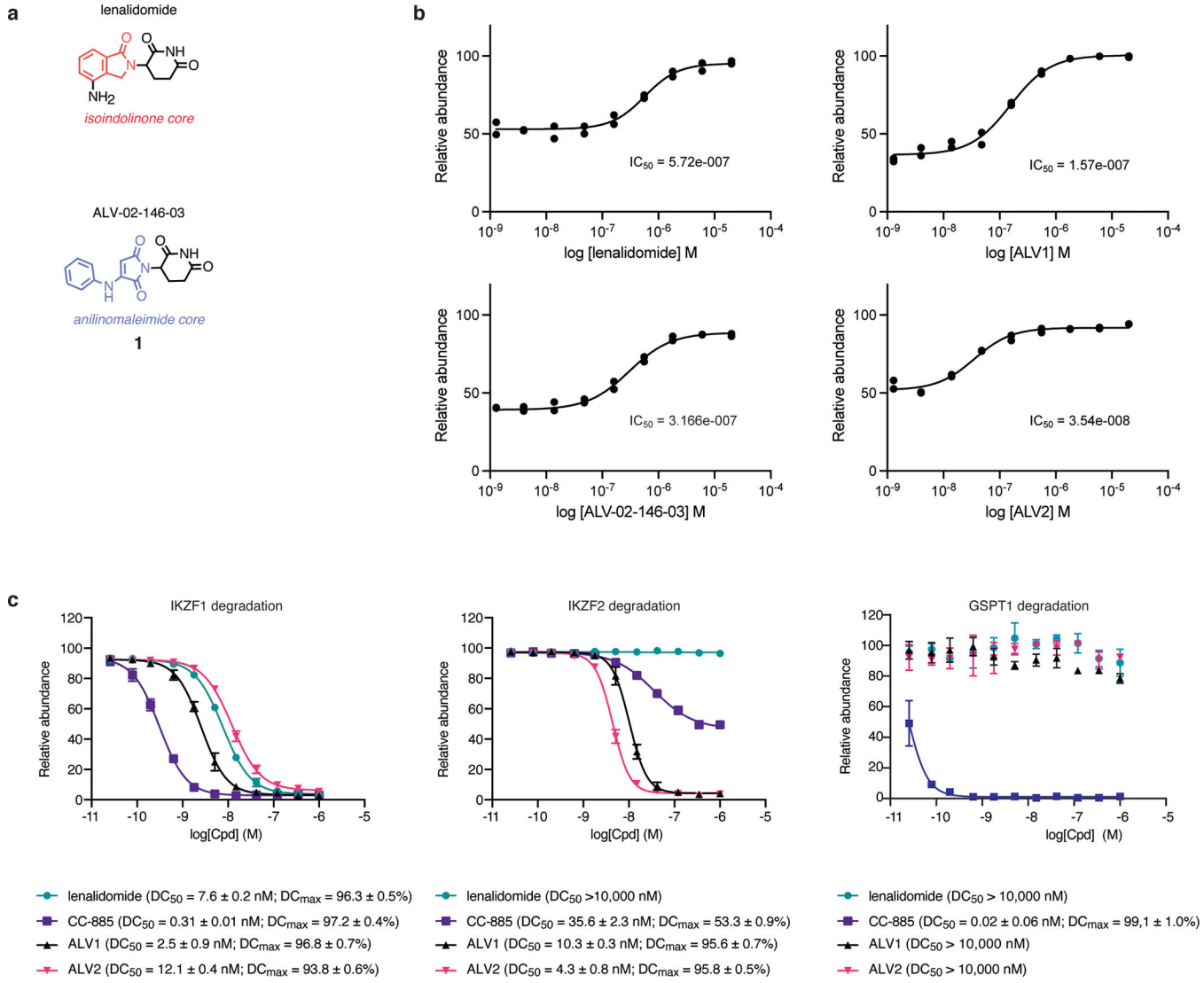

Extended Data Fig. 2. Novel imide analogs with anilinomaleimide cores bind CRBN in cells to induce Helios degradation

a, Chemical structure of lenalidomide and ALV-02–146-03 **(1)**, with the distinct isoindolinone and anilinomaleimide cores, respectively, highlighted. **b,** Cellular CRBN engagement assay for lenalidomide, ALV1, ALV2, and ALV-02–146-03. Data reported as n = 2 independent replicates. **c,** Quantitative assessment of cellular degradation using IKZF1-, IKZF2-, or GSPT1-EGFP reporter assay. Cells stably expressing EGFP fusions and mCherry were treated for 5h with increasing concentrations of ALV1, ALV2, CC-885 or lenalidomide, and EGFP and mCherry fluorescence was quantified, with half degradation constants (DC_{50}) and maximum percentage degradation (DC_{max}). Data reported as mean ± SD of n = 3 biologically independent samples and are representative of n = 2 independent experiments.

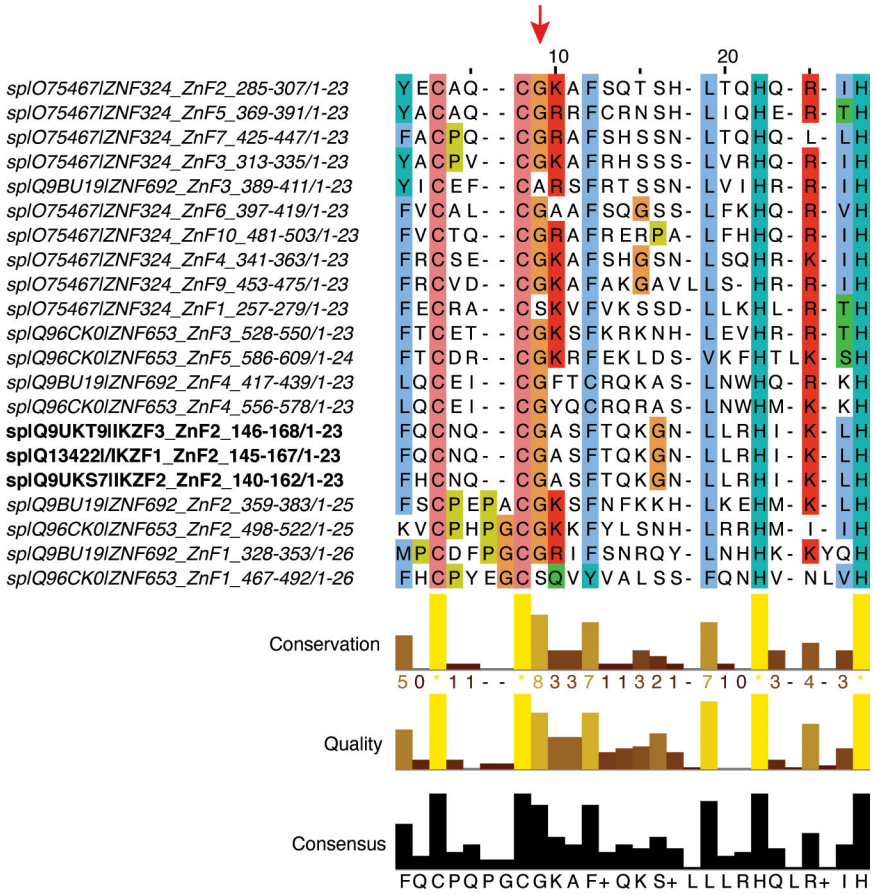

Extended Data Fig. 3. Selectivity profile of ALV1 and ALV2

Multiple sequence alignment of zinc finger domains of the proteins downregulated in Fig. 1f. The glycine residue indicated by the red arrow is a key determinant of imide dependent degradation and is present at least once in all downregulated proteins.

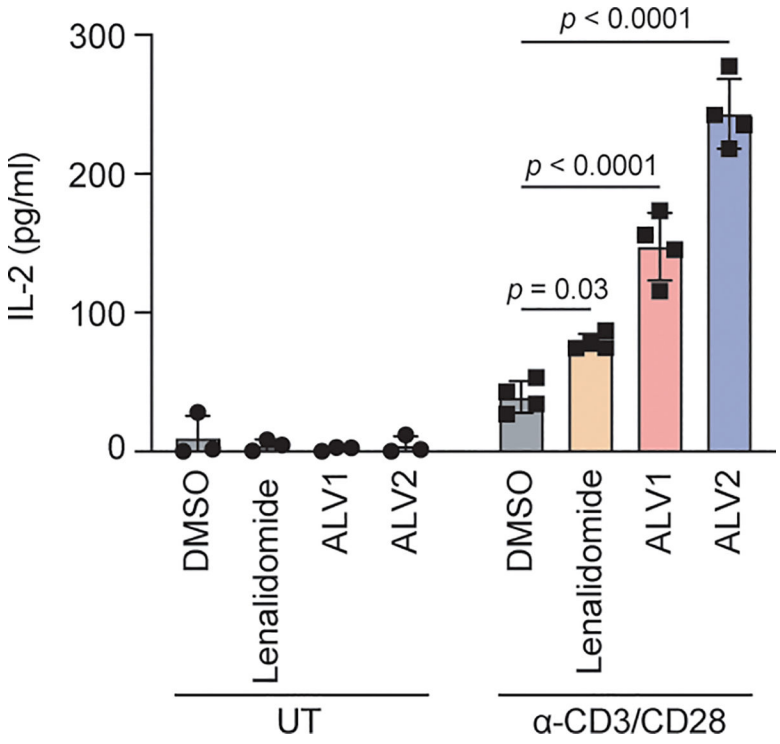

Extended Data Fig. 4. Helios degradation promotes IL-2 secretion

Jurkat cells were pre-treated with 1 μM of the indicated compounds for 18h and then activated with α-CD3/CD28 antibodies for 24h. Data is presented as mean ± SD of $n = 3$ (for untreated) and $n = 4$ (for stimulated) biologically independent samples and are representative of $n = 2$ independent experiments. Significance was assessed by two-way ANOVA with Bonferroni's correction for multiple comparisons.

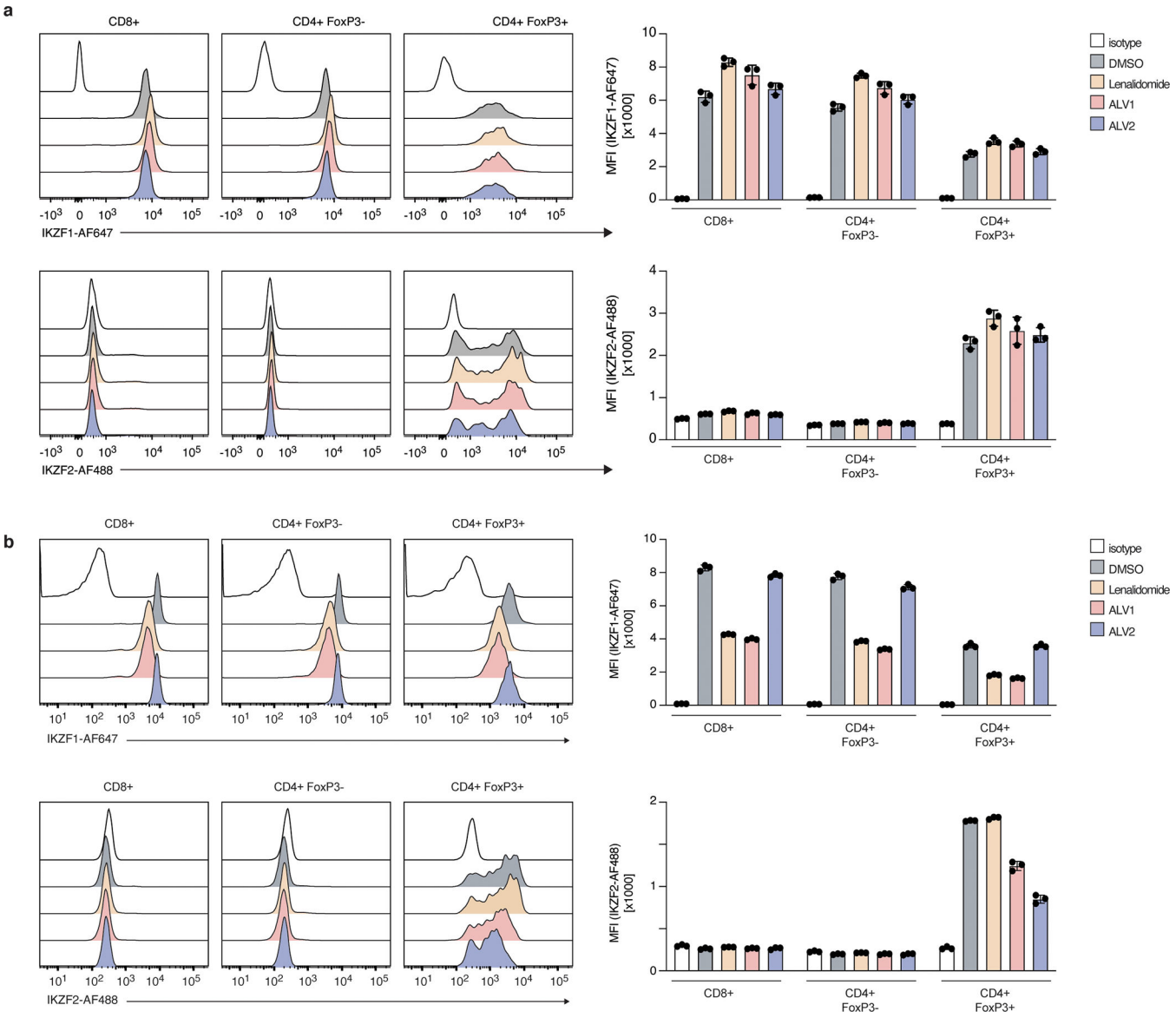

Extended Data Fig. 5. Acute Helios degradation in *Crbn*$^{I391V/I391V}$ but not wildtype murine Tregs

Representative histograms and quantification of **(a)** wildtype or **(b)** *Crbn*$^{I391V/I391V}$ splenocytes treated with 1 μM of the indicated compounds for 16h. Data is presented as mean ± SD of $n = 3$ biologically independent samples.

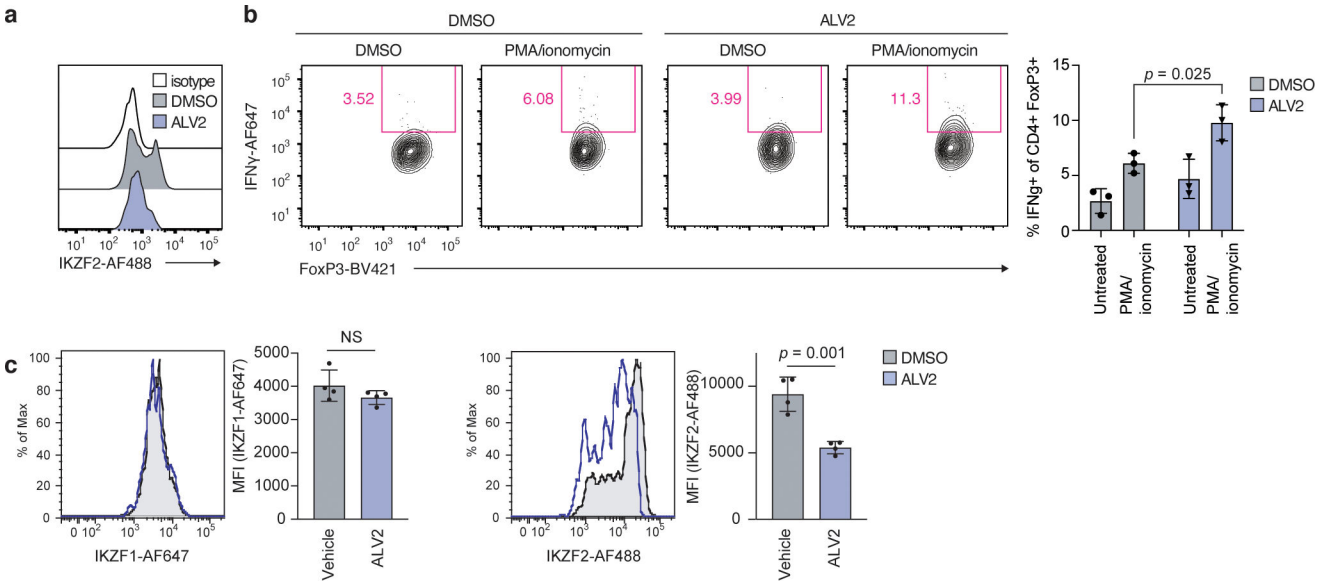

Extended Data Fig. 6. Acute Helios degradation in destabilizes murine Tregs

a, Histogram of Helios levels in CD4+ Foxp3+ Tregs after treatment *ex vivo* with ALV2 (2 μM) or DMSO vehicle in the presence of 5 ng/ml IL-2 + 20 ng/ml IL-4 for 4d. Data is representative of $n = 2$ biologically independent experiments. **b,** FACS plot and quantification of IFNγ+ CD4+ Foxp3+ Tregs after PMA/ionomycin stimulation. Data is presented as mean ± SD of $n = 3$ biologically independent samples and is representative of $n = 2$ independent experiments, and significance was assessed by two-way ANOVA with Bonferroni's correction for multiple comparisons. **c,** Representative histograms and quantification of Ikaros and Helios levels gated on splenic CD4+ FoxP3+ Tregs after treatment of $Crbn^{I391V/I391V}$ mice with vehicle (10% DMSO/50% PEG400/40% water) or ALV2 (100 mg/kg BID via intraperitoneal injection daily) for 7d. Data is presented as mean ± SD of $n = 4$ biologically independent mice, and p values are derived from a two-tailed t test.

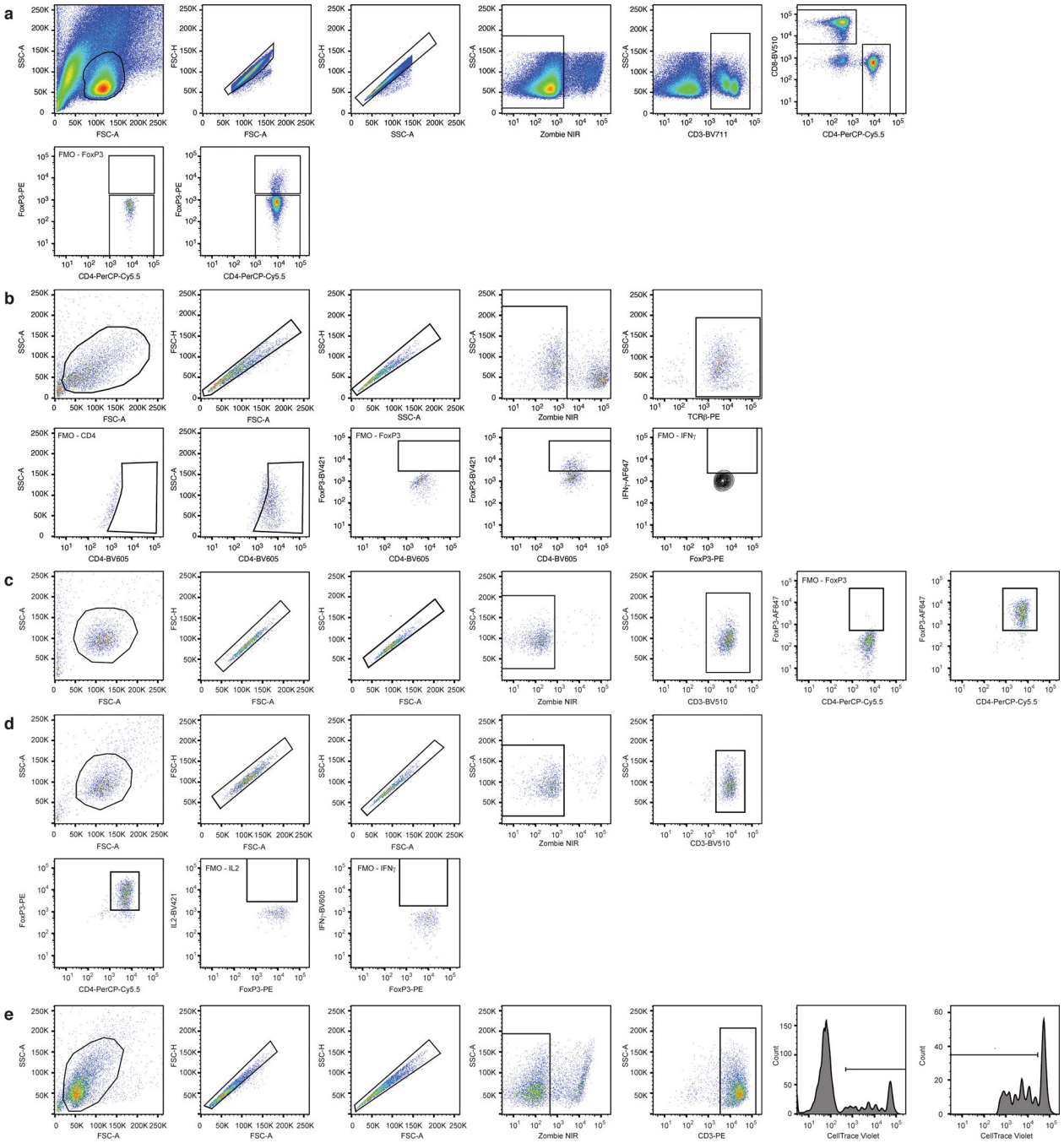

Extended Data Fig. 7. FACS gating strategy

Gating strategy used to identify different immune cell populations related to **(a)** Extended Data Fig. 5, 6c; **(b)** Extended Data Figure 6a, b; **(c)** Figure 3a; **(d)** Figure 4a, b; and **(e)** Figure 4c. FMO controls were used to set positive and negative gates as indicated.

Extended Data Table 1.

Data collection and refinement statistics.

	DDB1ΔB-CRBN-ALV1-IKZF2^{ZnF2}
Data collection	
Space group	$P2_1$
Cell dimensions	
a, *b*, *c* (Å)	151.80, 117.29, 196.71
α, β γ (°)	90, 97.30, 90,
Resolution (Å)	150.57 – 3.78 (3.86 – 3.78) *
R_{merge}	0.367 (1.813)
$I / \sigma I$	3.2 (0.7)
CC 1/2	0.988 (0.28)
Completeness (%)	98.2 (87.6)
Redundancy	4.6 (4.5)
Refinement	
Resolution (Å)	150.57–3.78
No. unique reflections	67299
R_{work} / R_{free} (%)	28.9 / 30.3
No. atoms	37535
Protein	37402
Ligand/ion	148
B-factors	
Protein	124.36
Ligand/ion	111.45
R.m.s. deviations	
Bond lengths (Å)	0.004
Bond angles (°)	0.70

* Values in parentheses are for highest-resolution shell.

Supplementary Material

Refer to Web version on PubMed Central for supplementary material.

Acknowledgments:

This work is based upon research conducted at the Northeastern Collaborative Access Team beamlines, which are funded by the National Institute of General Medical Sciences from the National Institutes of Health (P41 GM103403). The Pilatus 6M detector on 24-ID-C beam line is funded by a NIH-ORIP HEI grant (S10 RR029205). This research used resources of the Advanced Photon Source, a U.S. Department of Energy (DOE) Office of Science User Facility operated for the DOE Office of Science by Argonne National Laboratory under Contract No. DE-AC02–06CH11357. Software used in this project was curated by SBGrid[30].

Funding: The authors gratefully acknowledge the generous financial support of the following sources: NIH grant NCI R01CA214608 (grant to ESF), Damon Runyon Cancer Research Fellowship DRG-2270–16 (ESW), and the Damon Runyon-Rachleff Innovator Award DRR-50–18 (ESF).

Competing interests: NSG is an equity holder and scientific advisor for Syros, Soltego (board member), C4, B2S, Petra, Allorion, Inception, and Jengu. ESF is an equity holder and scientific advisor for C4 Therapeutics, Jengu

(board member), Neomorph and Civetta Therapeutics and is a consultant to Novartis, Sanofi, AbbVie, Pfizer, Astellas, EcoR1 capital and Deerfield. The Fischer lab receives or has received research funding from Novartis, Ajax, and Astellas not related to this work. ESW, ALV, RPN, JCY, KAD, NSG, and ESF are inventors on a patent covering the compounds described in this paper.

References

1. Sakaguchi S, Yamaguchi T, Nomura T & Ono M Regulatory T cells and immune tolerance. Cell 133, 775–787, doi:10.1016/j.cell.2008.05.009 (2008). [PubMed: 18510923]
2. Tanaka A & Sakaguchi S Regulatory T cells in cancer immunotherapy. Cell Res 27, 109–118, doi:10.1038/cr.2016.151 (2017). [PubMed: 27995907]
3. Onizuka S et al. Tumor rejection by in vivo administration of anti-CD25 (interleukin-2 receptor alpha) monoclonal antibody. Cancer Res 59, 3128–3133 (1999). [PubMed: 10397255]
4. Sakaguchi S Naturally arising CD4+ regulatory t cells for immunologic self-tolerance and negative control of immune responses. Annu Rev Immunol 22, 531–562, doi:10.1146/annurev.immunol.21.120601.141122 (2004). [PubMed: 15032588]
5. Nakagawa H et al. Instability of Helios-deficient Tregs is associated with conversion to a T-effector phenotype and enhanced antitumor immunity. Proc Natl Acad Sci U S A 113, 6248–6253, doi:10.1073/pnas.1604765113 (2016). [PubMed: 27185917]
6. Kim HJ et al. Stable inhibitory activity of regulatory T cells requires the transcription factor Helios. Science 350, 334–339, doi:10.1126/science.aad0616 (2015). [PubMed: 26472910]
7. Yates K, Bi K, Haining WN, Cantor H & Kim HJ Comparative transcriptome analysis reveals distinct genetic modules associated with Helios expression in intratumoral regulatory T cells. Proc Natl Acad Sci U S A 115, 2162–2167, doi:10.1073/pnas.1720447115 (2018). [PubMed: 29440380]
8. Kronke J et al. Lenalidomide causes selective degradation of IKZF1 and IKZF3 in multiple myeloma cells. Science 343, 301–305, doi:10.1126/science.1244851 (2014). [PubMed: 24292625]
9. Lu G et al. The myeloma drug lenalidomide promotes the cereblon-dependent destruction of Ikaros proteins. Science 343, 305–309, doi:10.1126/science.1244917 (2014). [PubMed: 24292623]
10. Kronke J et al. Lenalidomide induces ubiquitination and degradation of CK1alpha in del(5q) MDS. Nature 523, 183–188, doi:10.1038/nature14610 (2015). [PubMed: 26131937]
11. An J et al. pSILAC mass spectrometry reveals ZFP91 as IMiD-dependent substrate of the CRL4(CRBN) ubiquitin ligase. Nat Commun 8, 15398, doi:10.1038/ncomms15398 (2017). [PubMed: 28530236]
12. Donovan KA et al. Thalidomide promotes degradation of SALL4, a transcription factor implicated in Duane Radial Ray syndrome. Elife 7, doi:10.7554/eLife.38430 (2018).
13. Matyskiela ME et al. SALL4 mediates teratogenicity as a thalidomide-dependent cereblon substrate. Nat Chem Biol 14, 981–987, doi:10.1038/s41589-018-0129-x (2018). [PubMed: 30190590]
14. Matyskiela ME et al. A novel cereblon modulator recruits GSPT1 to the CRL4(CRBN) ubiquitin ligase. Nature 535, 252–257, doi:10.1038/nature18611 (2016). [PubMed: 27338790]
15. John LB & Ward AC The Ikaros gene family: transcriptional regulators of hematopoiesis and immunity. Mol Immunol 48, 1272–1278, doi:10.1016/j.molimm.2011.03.006 (2011). [PubMed: 21477865]
16. Fan Y & Lu D The Ikaros family of zinc-finger proteins. Acta Pharm Sin B 6, 513–521, doi:10.1016/j.apsb.2016.06.002 (2016). [PubMed: 27818917]
17. Powell CE et al. Selective Degradation of GSPT1 by Cereblon Modulators Identified via a Focused Combinatorial Library. ACS Chem Biol 15, 2722–2730, doi:10.1021/acschembio.0c00520 (2020). [PubMed: 32865967]
18. Petzold G, Fischer ES & Thoma NH Structural basis of lenalidomide-induced CK1alpha degradation by the CRL4(CRBN) ubiquitin ligase. Nature 532, 127–130, doi:10.1038/nature16979 (2016). [PubMed: 26909574]
19. Nowak RP et al. Plasticity in binding confers selectivity in ligand-induced protein degradation. Nat Chem Biol 14, 706–714, doi:10.1038/s41589-018-0055-y (2018). [PubMed: 29892083]

20. Sievers QL et al. Defining the human C2H2 zinc finger degrome targeted by thalidomide analogs through CRBN. Science 362, doi:10.1126/science.aat0572 (2018).
21. Baine I, Basu S, Ames R, Sellers RS & Macian F Helios induces epigenetic silencing of IL2 gene expression in regulatory T cells. J Immunol 190, 1008–1016, doi:10.4049/jimmunol.1200792 (2013). [PubMed: 23275607]
22. Haslett PA, Corral LG, Albert M & Kaplan G Thalidomide costimulates primary human T lymphocytes, preferentially inducing proliferation, cytokine production, and cytotoxic responses in the CD8+ subset. J Exp Med 187, 1885–1892, doi:10.1084/jem.187.11.1885 (1998). [PubMed: 9607928]
23. Gandhi AK et al. Immunomodulatory agents lenalidomide and pomalidomide co-stimulate T cells by inducing degradation of T cell repressors Ikaros and Aiolos via modulation of the E3 ubiquitin ligase complex CRL4(CRBN.). Br J Haematol 164, 811–821, doi:10.1111/bjh.12708 (2014). [PubMed: 24328678]
24. Corral LG et al. Differential cytokine modulation and T cell activation by two distinct classes of thalidomide analogues that are potent inhibitors of TNF-alpha. J Immunol 163, 380–386 (1999). [PubMed: 10384139]
25. Fink EC et al. Crbn (I391V) is sufficient to confer in vivo sensitivity to thalidomide and its derivatives in mice. Blood 132, 1535–1544, doi:10.1182/blood-2018-05-852798 (2018). [PubMed: 30064974]
26. Gokhale AS, Gangaplara A, Lopez-Occasio M, Thornton AM & Shevach EM Selective deletion of Eos (Ikzf4) in T-regulatory cells leads to loss of suppressive function and development of systemic autoimmunity. J Autoimmun 105, 102300, doi:10.1016/j.jaut.2019.06.011 (2019). [PubMed: 31296356]
27. Pan F et al. Eos mediates Foxp3-dependent gene silencing in CD4+ regulatory T cells. Science 325, 1142–1146, doi:10.1126/science.1176077 (2009). [PubMed: 19696312]
28. Donovan KA et al. Mapping the Degradable Kinome Provides a Resource for Expedited Degrader Development. Cell 183, 1714–1731 e1710, doi:10.1016/j.cell.2020.10.038 (2020). [PubMed: 33275901]
29. Sebastian M et al. Helios Controls a Limited Subset of Regulatory T Cell Functions. J Immunol 196, 144–155, doi:10.4049/jimmunol.1501704 (2016). [PubMed: 26582951]
30. Morin A et al. Collaboration gets the most out of software. eLife 2, e01456, doi:10.7554/eLife.01456 (2013). [PubMed: 24040512]

Methods Only References

31. Abdulrahman W et al. A set of baculovirus transfer vectors for screening of affinity tags and parallel expression strategies. Anal Biochem 385, 383–385, doi:10.1016/j.ab.2008.10.044 (2009). [PubMed: 19061853]
32. Zakeri B et al. Peptide tag forming a rapid covalent bond to a protein, through engineering a bacterial adhesin. Proc Natl Acad Sci U S A 109, E690–697, doi:10.1073/pnas.1115485109 (2012). [PubMed: 22366317]
33. Cavadini S et al. Cullin-RING ubiquitin E3 ligase regulation by the COP9 signalosome. Nature 531, 598–603, doi:10.1038/nature17416 (2016). [PubMed: 27029275]
34. McCoy AJ et al. Phasertng: directed acyclic graphs for crystallographic phasing. Acta Crystallogr D Struct Biol 77, 1–10, doi:10.1107/S2059798320014746 (2021). [PubMed: 33404520]
35. Afonine PV et al. Towards automated crystallographic structure refinement with phenix.refine. Acta Crystallogr D Biol Crystallogr 68, 352–367, doi:10.1107/S0907444912001308 (2012). [PubMed: 22505256]
36. Smart OS et al. Exploiting structure similarity in refinement: automated NCS and target-structure restraints in BUSTER. Acta Crystallogr D Biol Crystallogr 68, 368–380, doi:10.1107/S0907444911056058 (2012). [PubMed: 22505257]
37. Chen VB et al. MolProbity: all-atom structure validation for macromolecular crystallography. Acta Crystallogr D Biol Crystallogr 66, 12–21, doi:10.1107/S0907444909042073 (2010). [PubMed: 20057044]

38. Carpenter AE et al. CellProfiler: image analysis software for identifying and quantifying cell phenotypes. Genome Biol 7, R100, doi:10.1186/gb-2006-7-10-r100 (2006). [PubMed: 17076895]

39. McAlister GC et al. MultiNotch MS3 enables accurate, sensitive, and multiplexed detection of differential expression across cancer cell line proteomes. Analytical chemistry 86, 7150–7158, doi:10.1021/ac502040v (2014). [PubMed: 24927332]

40. R: A language and environment for statistical computing. (R Foundation for Statistical Computing, 2014).

41. Ritchie ME et al. limma powers differential expression analyses for RNA-sequencing and microarray studies. Nucleic Acids Res 43, e47, doi:10.1093/nar/gkv007 (2015). [PubMed: 25605792]

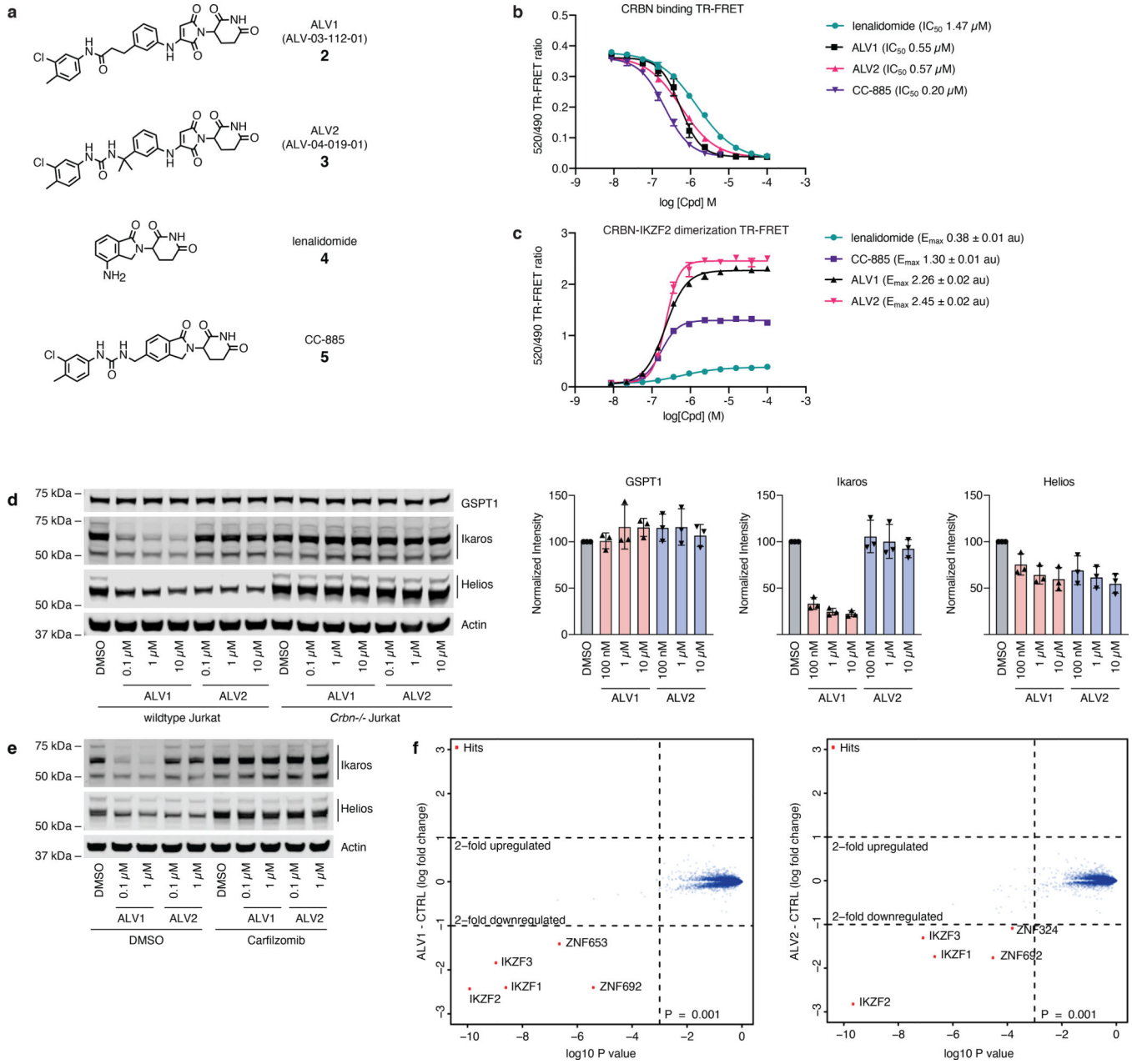

Figure 1: Novel anilinomaleimides induce Helios degradation

a, Chemical structures of ALV1, ALV2, lenalidomide, and CC-885. **b**, CRBN-binding TR-FRET assay. Displacement of BODIPY-lenalidomide tracer by titration of lenalidomide, ALV1 and ALV2 to DDB1ΔB-$CRBN_{biotinylated}$ and Tb-streptavidin. Data is presented as mean ± SD of $n = 3$ biologically independent samples. **c**, CRBN-IKZF2 TR-FRET assay. Titration of lenalidomide, CC-885, ALV1 or ALV2 to DDB1ΔB-$CRBN_{SPYCATCHER-BODIPY}$, Terbium-Streptavidin and biotinylated IKZF2. Data is presented as mean ± SD of $n = 3$ biologically independent samples and is representative of $n = 3$ independent experiments. **d**, Representative immunoblots and quantification from $n = 3$ independent experiments of wildtype or *Crbn−/−* Jurkat cells treated as indicated for 4h. **e**,

Immunoblots from Jurkat cells co-treated with carfilzomib (1 μM) and the indicated compounds for 4h. Data is representative of two independent experiments. **f,** Quantitative proteomics profiles (7972 total proteins) of wildtype Jurkat cells treated for 4h with 1 μM of ALV1 or ALV2. Significant changes were assessed using a moderated t-test as implemented in Bioconductor's Limma package. Uncropped gels for **d, e** are included as Source Data - Figure 1.

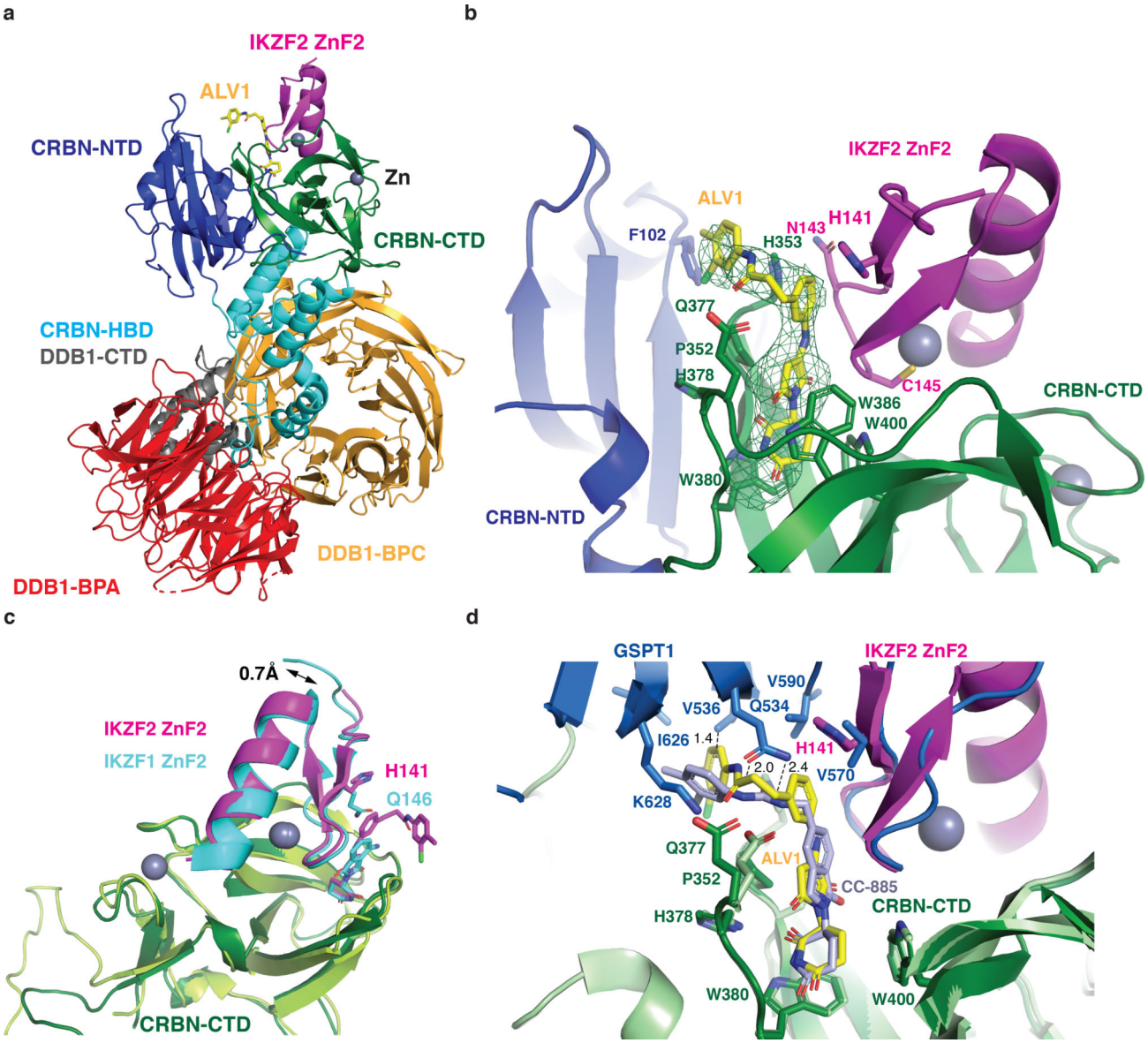

Figure 2: ALV1 accommodates key histidine 141 residue of IKZF2

a, Cartoon representation of DDB1ΔB-CRBN-ALV1-IKZF2^{ZnF2} highlighting the domain architecture. **b**, CRBN ALV1 binding site. The ALV1 F_o-F_c map contoured at 3.0 σ is shown as green mesh. **c**, Overlay of IKZF1^{ZnF1} (PDB: 6H0F) and IKZF2^{ZnF2} based on structure alignment of CTD of CRBN reveals 0.7 Å translation between the zinc fingers. IKZF2 H141 and corresponding IKZF1 Q146 residues are shown in stick representation. **d**, Overlay of the CC-885-GSPT1 complex (PDB: 5HXB) with the ALV1-IKZF2^{ZnF2} complex. Distances between GSPT1 Q534, V536 and ALV molecules are shown with dashed lines and measured in Å.

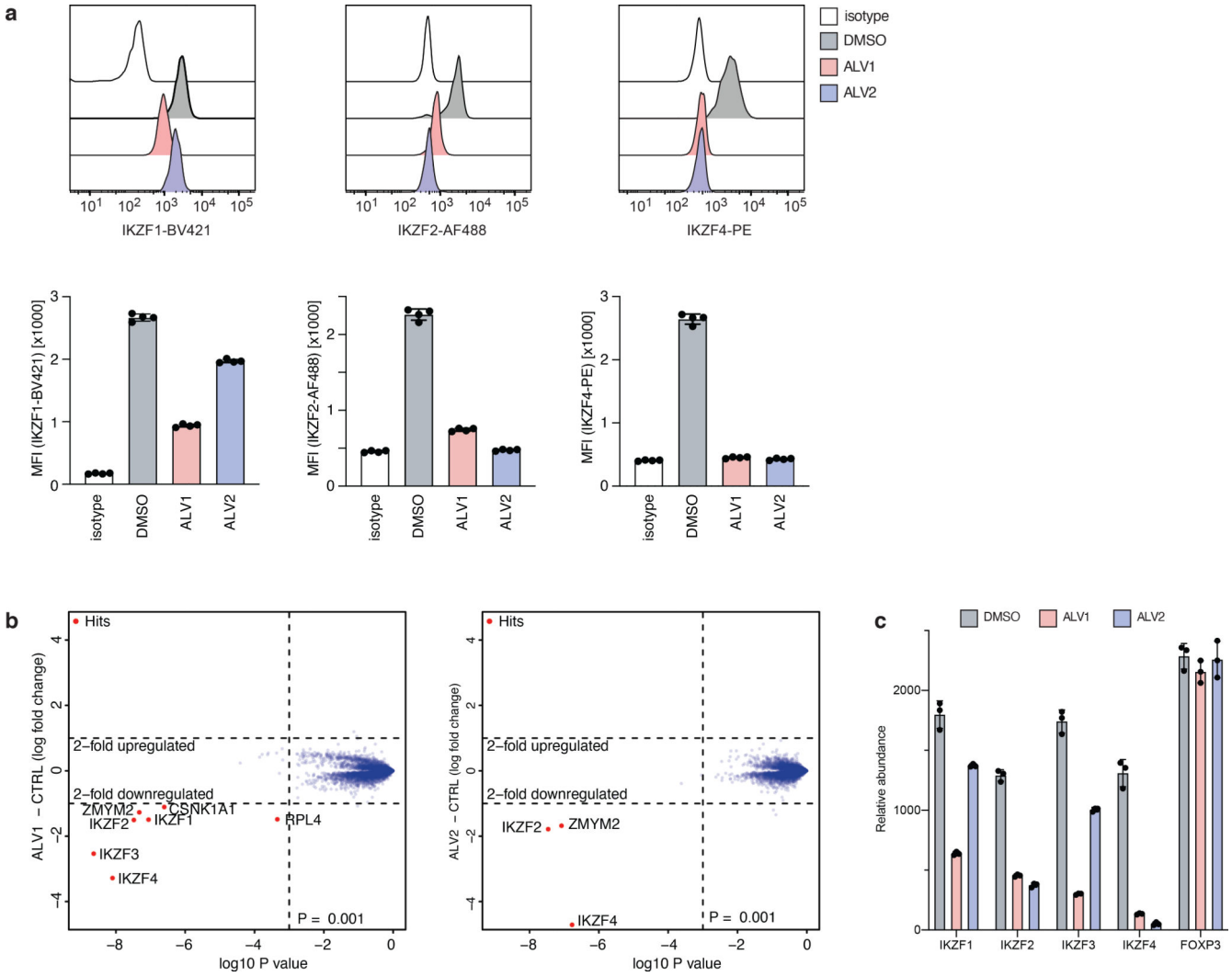

Figure 3: Acute degradation of Ikaros family transcription factors in human Tregs

a, Representative histograms and quantification of *ex vivo* expanded human Tregs treated with 1 μM of the indicated compounds for 24h. Data is presented as mean ± SD of $n = 4$ biologically independent samples and is representative of $n = 3$ independent experiments. **b,** Quantitative proteomics profiles (6808 total proteins) of human Tregs treated for 4h with 1 μM of ALV1 or ALV2. Significant changes were assessed using a moderated t-test as implemented in Bioconductor's Limma package. **c,** Relative abundance of indicated transcription factors in human Tregs treated for 4h with 1 μM of ALV1 or ALV2. Data is presented as mean ± SD of $n = 3$ biologically independent samples.

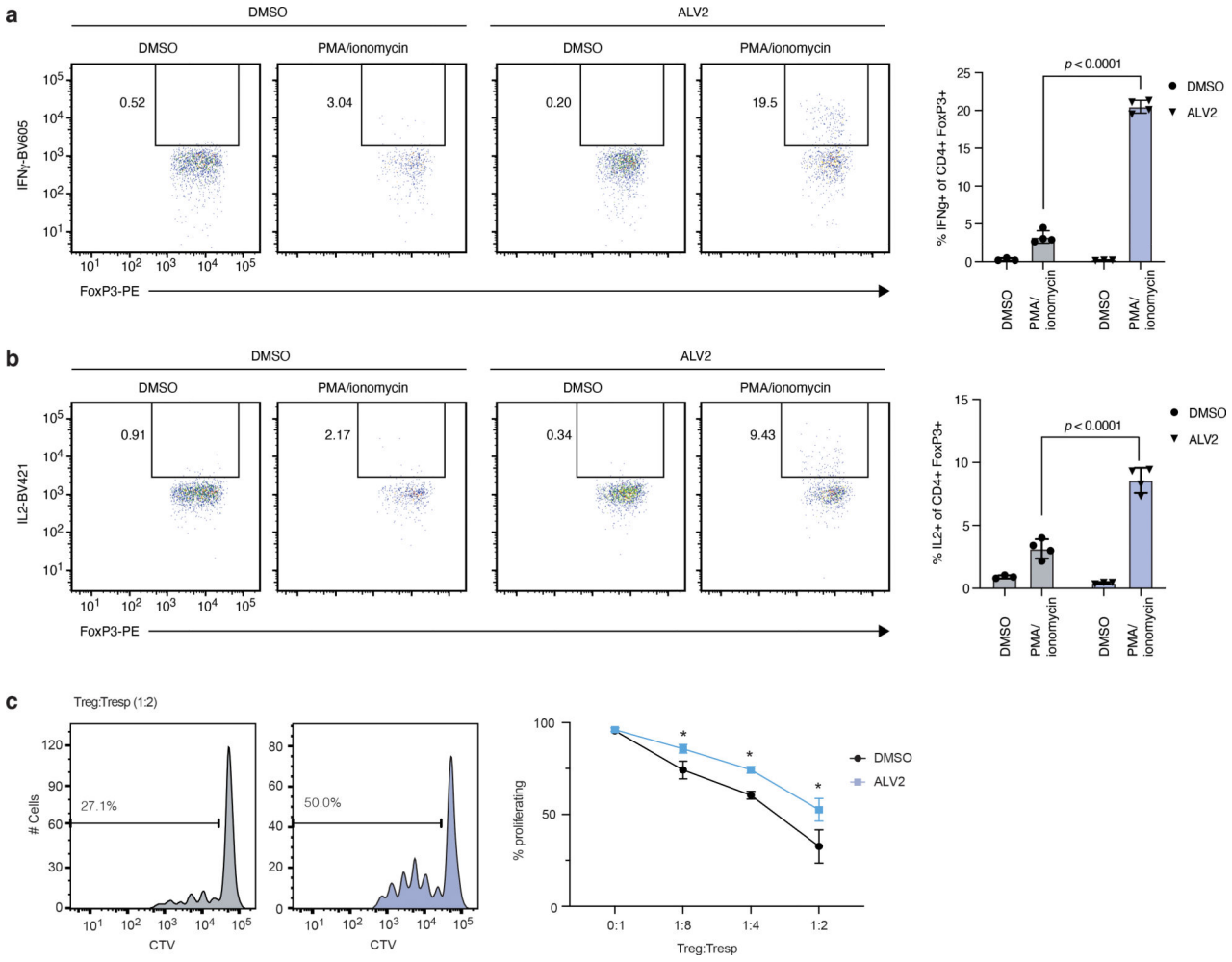

Figure 4. Pharmacological degradation of Helios destabilizes human Tregs *ex vivo*

Representative FACS plots and quantification of **(a)** % IL2+ or **(b)** % IFNγ+ cells within CD4+ Foxp3+ Tregs after PMA/ionomycin stimulation. Data is presented as mean ± SD of $n = 4$ biologically independent samples and is representative of $n = 3$ independent experiments. Significance was assessed by two-way ANOVA with Bonferroni's correction for multiple comparisons. **c,** Representative cell division profiles and quantification of proliferating CD3+ Tresp cells incubated with hTregs and ALV2 or vehicle control. Data is presented as mean ± SD of $n = 4$ biologically independent samples and is representative of $n = 2$ independent experiments. Significance was assessed by two-way ANOVA with Bonferroni's correction for multiple comparisons (1:8, $p = 0.0048$; 1:4, $p = 0.0008$; 1:2, $p < 0.0001$).